SceneComplete: Open-World 3D Scene Completion in Complex Real World Environments for Robot Manipulation

Aditya Agarwal¹, Gaurav Singh², Bipasha Sen¹, Tomás Lozano-Pérez¹, Leslie Pack Kaelbling¹

¹MIT CSAIL, ²IIIT-Hyderabad



Fig. 1: SceneComplete (a) takes as input a single RGB-D image of a given scene, visualized here as a point cloud; (b) produces high-quality fully completed, accurately segmented object meshes in scenes with substantial occlusion and novel objects; and (c) enables downstream dexterous manipulation that requires accurate complete shape information.

Abstract—Careful robot manipulation in every-day cluttered environments requires an accurate understanding of the 3D scene, in order to grasp and place objects stably and reliably and to avoid mistakenly colliding with other objects. In general, we must construct such a 3D interpretation of a complex scene based on limited input, such as a single RGB-D image. We describe SceneComplete, a system for constructing a complete, segmented, 3D model of a scene from a single view. It provides a novel pipeline for composing generalpurpose pretrained perception modules (vision-language, segmentation, image-inpainting, image-to-3D, and pose-estimation) to obtain high-accuracy results. We demonstrate its accuracy and effectiveness with respect to ground-truth models in a large benchmark dataset and show that its accurate wholeobject reconstruction enables robust grasp proposal generation, including for a dexterous hand.

I. INTRODUCTION

As manipulation robots move from constrained environments such as factories to open-world environments such as homes and hospitals, they must be able to construct representations of their environment that enable robust, careful manipulation. Such representations need to individuate objects and characterize their shapes, so that the robot can reliably select stable grasps and placements for individual objects so that it can manipulate them without unwanted collisions. These representations must generally be constructed from limited input, such as a single RGB-D image. The problem is fundamentally ill-posed, but we are now in a position to address it using strong prior knowledge that has been learned by vision foundation models.

In this paper, we propose a solution to this open-world scene completion problem in the form of a perception pipeline, *SceneComplete*. It combines multiple large pretrained vision models into a system that takes a single RGB-D image as input and predicts as output a completed scene, consisting of a set of meshes for all the visible objects, including those that are partially occluded, Crucially, it makes no assumptions about the categories of the objects, their arrangement, or the camera viewpoint. It is constructed from multiple highly capable pre-trained perception components: a vision-language model (VLM) for identifying and generating short descriptions of the objects in a scene, a textgrounded image-segmentation model for localizing objects in the image, a 2D image-inpainting model for predicting the appearance of occluded parts of objects, an image-to-3D model for generating complete object meshes, and visual descriptor and pose-estimation modules to aid in composing individual predicted meshes into a final scene. None of these components can individually solve the problem, but in combination they provide robust object-centric interpretation of complex images, producing a segmented set of object meshes that are suitable for robot planning and manipulation.

As far as we know, this is the first system to support full-scene reconstruction from a single real-world RBG-D input in cluttered, occluded scenes with no assumptions about object categories. Many previous systems [1]–[11] have addressed simpler versions of this problem, with various combinations of known object categories, idealized sensory input, or lack of clutter. Handling the full generality of this problem class adds substantial difficulty to the problem.

To demonstrate the effectiveness of *SceneComplete*, we conduct extensive quantitative and qualitative evaluations on real-world tabletop scenes. Our quantitative evaluations are on the Graspnet-1B dataset [12], which consists of heavily cluttered tabletop scenes. In these scenarios, accurately predicting the full scene—including partially occluded objects—is crucial for stable grasping, collision-free

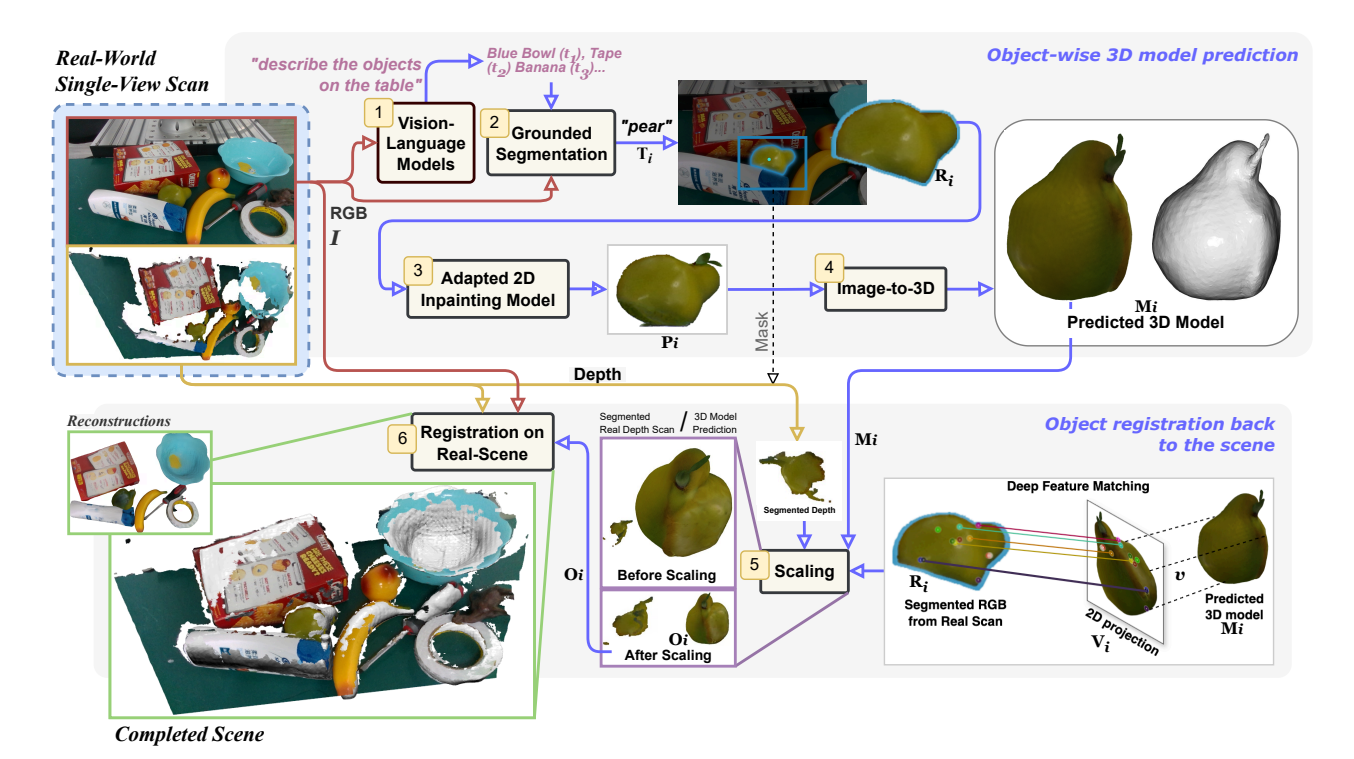


Fig. 2: Overview of the SceneComplete pipeline. Starting from a single RGB-D input, the system produces a set of object meshes registered with the input 3D scan, yielding a complete 3D scene reconstruction. The pipeline consists of six key phases: (1) An RGB image is fed into a vision-language model to enumerate and describe objects, (2) object descriptions and the RGB image are processed by a grounded segmentation model to generate object masks, (3) occluded regions are completed via image inpainting model adapted to output single fully observable objects on a white background, (4) the inpainted 2D images are passed into an image-to-3D model to produce object meshes, (5) object meshes are scaled according to the segmented partial point cloud, and (6) mesh poses are adjusted within the 3D coordinate frame of the original scan using 6DOF pose estimation. Each step leverages pre-trained open world large vision models, enabling scalability and benefiting from future model improvements.

motion with an object in the hand, and reliable placing. We further illustrate the utility of our shape-reconstruction methods by using them as input to parallel-jaw [13] and dexterous grasping [14] proposal methods, the latter being especially sensitive to the detailed shape of the entire object.

II. METHOD

Figure 2 illustrates the overall design of *SceneComplete*. It takes a single RGB-D image as input and produces a set of object meshes that are registered with the input 3D scan. The objective is to provide an accurate 3D reconstruction of the scene, in terms of segmentation into rigid components, and the shape of each component, expressed as a mesh. It operates in the following phases:

- The RGB image is presented to a vision-language model, which is prompted to enumerate and describe the objects in the scene. (Sec. II-A)
- 2) These object descriptions, together with the RGB image, are input to a grounded segmentation model, which produces, for each object description, an image mask indicating the region the object occurs in. (Sec. II-A)
- 3) To handle occlusion, for each object, we mask out all other objects, and use an image-inpainting model to complete the 2D image of that object. (Sec. II-B)
- 4) Now, for each object, we have a 2D image corresponding to just that object, which we pass into an Image-to-

- 3D model, which produces a high-quality textured mesh for the object, consistent with the image. (Sec. II-C)
- 5) The resulting object mesh has an arbitrary orientation, translation, and scale. For each object, we take the mesh and its associated image mask and partial point cloud (obtained in step 3) and determine an appropriate scale by finding correspondences and then solving for an appropriate scale. (Sec. II-D)
- 6) Finally, we determine an appropriate pose for each new mesh in the 3D coordinate frame of the original depth image using a 6DOF pose-estimation model. (Sec. II-E)

Importantly, each of these steps makes use of existing pretrained open-world visual-processing models, with almost no additional training (we have to do a small amount of lowrank adaptation of the inpainting model). This means that, as improved models become available for each of these tasks, as they inevitably will, we will be able to immediately profit from these improvements.

We describe each process in detail in the following subsections.

A. Prompting and segmentation

We begin by using a vision-language model to determine the number and basic description of objects in the scene. In our implementation, we pass the RGB image I into ChatGPT-40 [15] with the prompt "describe the objects in the image with their generic name and color as prompts in a list. No description." It produces a text response from which we extract a list t_1, \ldots, t_n of text descriptions of objects. For example, in the example shown in Fig. 2, it returns "Blue Bowl, Tape, Banana" and so on.

Next, we obtain an image mask for each object. For each text description t_i , we prompt a segmentation model (in our implementation, GroundedSam [16]) using t_i on image I and obtain a candidate set of pairs of masks and confidence values. For example, the prompt "a pear" might return multiple useful masks in a scene with two pears; in other cases, some of the masks will be unhelpful (and hopefully low-confidence). We use the confidence values to greedily select a set of non-overlapping masks, and associate each mask with the text prompt that generated it, producing the set $(R_1, T_1), \ldots, (R_N, T_N)$, R and T denoting the masks and prompts, respectively, for N objects in the scene. Our objective now is to compute a mesh corresponding to each of these hypothesized objects.

B. Image Inpainting



Fig. 3: In the image inpainting module, occluded objects (blue borders) are transformed into single fully observable objects.

As illustrated in the Fig. 3, the objects represented by the masks in $(R_1, T_1), \ldots, (R_N, T_N)$ could be partially occluded by other objects in the scene. In this step, we use an image inpainting algorithm to fill in the occluded parts of each object's image. This is important for the next step of predicting a 3D mesh, because the image-to-3D models only perform reliably with a complete view of the object. Fig. 4 (a) illustrates the bad effects of attempting reconstruction from an incomplete image.

In our implementation we begin with BrushNet [17], which takes an image with explicitly masked out regions and a text prompt, and produces a completed image, with the masked portions filled in. So for each (R_i, T_i) pair, we begin by constructing an image I_i with just the segmented object region R_i on a white background. Then we construct an inpainting mask consisting of the union of the regions R_j for $j \neq i$. Finally we query Brushnet with I_i , $\cup_{j \neq i} R_j$, and T_i and obtain an inpainted image P_i of the completed object on a white background.

However, we observed that, out of the box, BrushNet occasionally synthesized additional objects in the occluded areas, as shown in Fig. 4 (b), possibly due to the "artistic" data set on which it was trained. To improve this behavior, we adapt BrushNet to full, single objects. It is important to note that, even though we want to adapt BrushNet to single fully observed objects, we want to retain the open world capabilities of the model. To achieve this, we use Low-Rank Adaptation (LoRA) [18] on its learnable layers with the

PEFT [19] method, targeting domain-specific improvements on the tabletop YCB dataset [20]. LoRA is an effective method for adapting pretrained models to domain-specific outputs while retaining the inherent generalization of the models. To perform this adaptation, we project the different 3D YCB object meshes from arbitrary poses on a white background and add random brush masks for inpainting as suggested by BrushNet. The adapted model allows us to reliably inpaint individual occluded objects, including those from categories not in the adaptation dataset,

C. Image-to-3D models for object reconstruction

At this point, we have, for each object, a fully observed object image P_i on a white background. The next step is to generate a 3D mesh model for the object. Although methods exist for operating directly on the point-cloud generated from the depth channel of the RGB-D image, the depth information is often very low-resolution and noisy, so these depth-only models tend to be highly tuned to specific categories [2], [6], [7], [21], [22] and viewpoints as shown in Fig. 7. There have been substantial recent improvements in RGB-only methods, which take advantage of the high quality of the RGB signal and enormous amounts of available training data [23]–[29].

For RGB image as inputs, one option is to use methods that optimize a 3D mesh through differentiable rendering [30]–[34]. Although these models have impressive open world results, they have substantial computational cost. On the other hand, feed-forward methods such as InstantMesh [29] that directly map a single-view RGB image into a 3D mesh are highly accurate, open world, and computationally inexpensive at the time of inference. For these reasons, we use InstantMesh, providing each image P_i as input and obtaining a complete textured 3D mesh M_i as output. The resulting meshes are produced in an arbitrary orientation, at an arbitrary scale, so more work remains to be done, as explained in the subsequent subsections.

D. Mesh Scaling using Dense Correspondence Matching

The next step is to rescale the meshes M_i , using a point-cloud constructed from the region R_i to determine the scale as follows:

- Using the default viewpoint v from InstantMesh, generate an image V_i as a 2D projection of mesh M_i .
- Following [35], find dense visual descriptors of the segmented original image, R_i and the projected image, V_i , using a pre-trained vision transformer (we use [36], [37]). In our observation, v is usually close to the viewpoint from which R_i was rendered. This enables us to obtain matching visual descriptors across R_i and V_i .
- Generate dense pixel-wise correspondences between the descriptor images, so that we have a set of pairs (R_i^j, V_i^j) where R_i^j is a pixel in the original image of the object and V_i^j is a pixel in the synthesized view.
- Map these correspondences into 3D, to obtain a pair $(R_i^{j'}, V_i^{j'})$ of points in 3D. (Note that these point sets

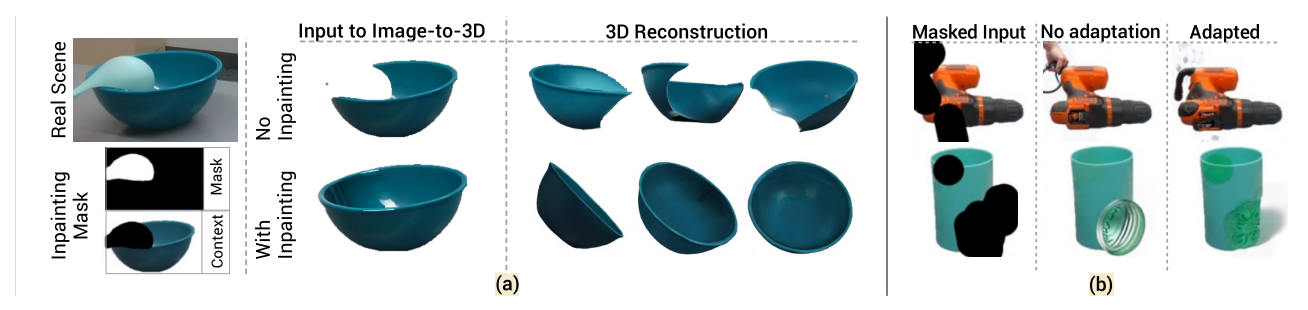


Fig. 4: (a) The impact of inpainting on image-to-3D reconstruction. Without inpainting (top), the image-to-3D model generates incomplete meshes. Inpainting (bottom) fills in occluded parts, producing accurate 3D reconstructions. (b) Comparison of inpainting models. Unadapted BrushNet (middle) introduces artifacts, while the adapted version (right) correctly inpaints occluded objects producing a single fully observable object, improving 3D predictions for robotic manipulation in cluttered scenes.

may not yet be aligned in 3D—we address that problem in the next step.)

- Center each resulting 3D cloud, compute the average Euclidean distance from the points to the centroid in each one, and compute the ratio of these values as the scale factor.
- Apply the scale factor to the mesh M_i to put it in the same scale as the original point cloud to obtain O_i as shown in Fig. 2-(5).

E. 6D Object Pose Estimation and Registration

Now, we have, for each object, an appropriately scaled mesh O_i , and we need to reconstruct the entire scene. To do this, we need to find a 6DOF transform for each mesh that causes it to register well with the observed point cloud. For this task, we use FoundationPose [38], a robust object-pose estimation method designed to operate without being limited to specific object categories. We use its model-based mode, which takes as input a partial point-cloud derived from region R_i of the input RGB-D image and an appropriately scaled textured object mesh O_i , and returns a 6DOF transform τ_i mapping O_i into the coordinate frame of the point cloud.

As a result of this process, we have a set of pairs (O_i, τ_i) , where each O_i is a textured complete mesh for object i and τ_i is a pose for that mesh in the camera coordinate frame. This scene reconstruction provides a highly general representation for a wide variety of downstream object-manipulation tasks. Accurate reconstructions of unobserved parts of objects enables a wide variety of manipulation operations, including many types of robust grasping, moving safely in cluttered but unobserved parts of the scene, moving safely when holding a grasped object, packing objects into boxes, etc.

III. EXPERIMENTS

We evaluate the accuracy and utility of *SceneComplete* in three different regimes:

- Quantitative evaluation of reconstruction accuracy on a large-scale dataset of tabletop scenes with RGB-D scans captured using a Realsense D435 camera, GraspNet-1B [12], against the ground-truth object models and poses.
- Qualitative evaluation of reconstruction on a smallerscale dataset of tabletop scenes with RGB-D images

(also collected with a Realsense D435) but using objects in our lab that have little chance of having appeared in the training of any of the models in the system.

Task-driven evaluation of reconstruction by demonstrating that the reconstructed object models are sufficiently accurate to enable grasp proposals for a multi-fingered hand, which depends on having a good estimate of the entire object shape.

We additionally observe that the runtime of the current implementation of *SceneComplete* is about 30s per object; we expect this to improve with advances in models and GPUs.

There are no existing methods that solve the same problem, so we compare against an ablation of *SceneComplete*, which uses the same pipeline, but instead of using image-to-3D shape completion, we use the convex-hull of the partial point-cloud associated with each segmented image region R_i .

We believe that our results illustrate the ability of *SceneComplete* to:

- produce highly accurate reconstructions of unobserved parts of a scene,
- operate in cluttered scenes with substantial occlusion,
- generalize "zero-shot" to previously unseen object types, and
- provide important spatial information that supports collision-free manipulation and multi-fingered grasping.

A. Scene Reconstruction

We begin by evaluating the ability of *SceneComplete* to generate highly accurate scene reconstructions, using the GraspNet-1B dataset [12]. This dataset is particularly suitable for our evaluation due to its large collection of 190 cluttered tabletop scenes, featuring a diverse array of 88 unique objects in various configurations. It includes ground-truth 3D object models and poses for each scene, as well as real RGB-D images of the scenes.

Our primary reconstruction evaluation metric is based on comparing the ground-truth meshes with those produced by the *SceneComplete*. Let U^* be the union of the volumes meshes of the ground-truth objects and let \widehat{U} be the union of the volumes of the meshes produced by a reconstruction algorithm. Then the intersection-over-union metric is

$$IoU(U^*, \widehat{U}) = \frac{U^* \cap \widehat{U}}{U^* \cup \widehat{U}} .$$

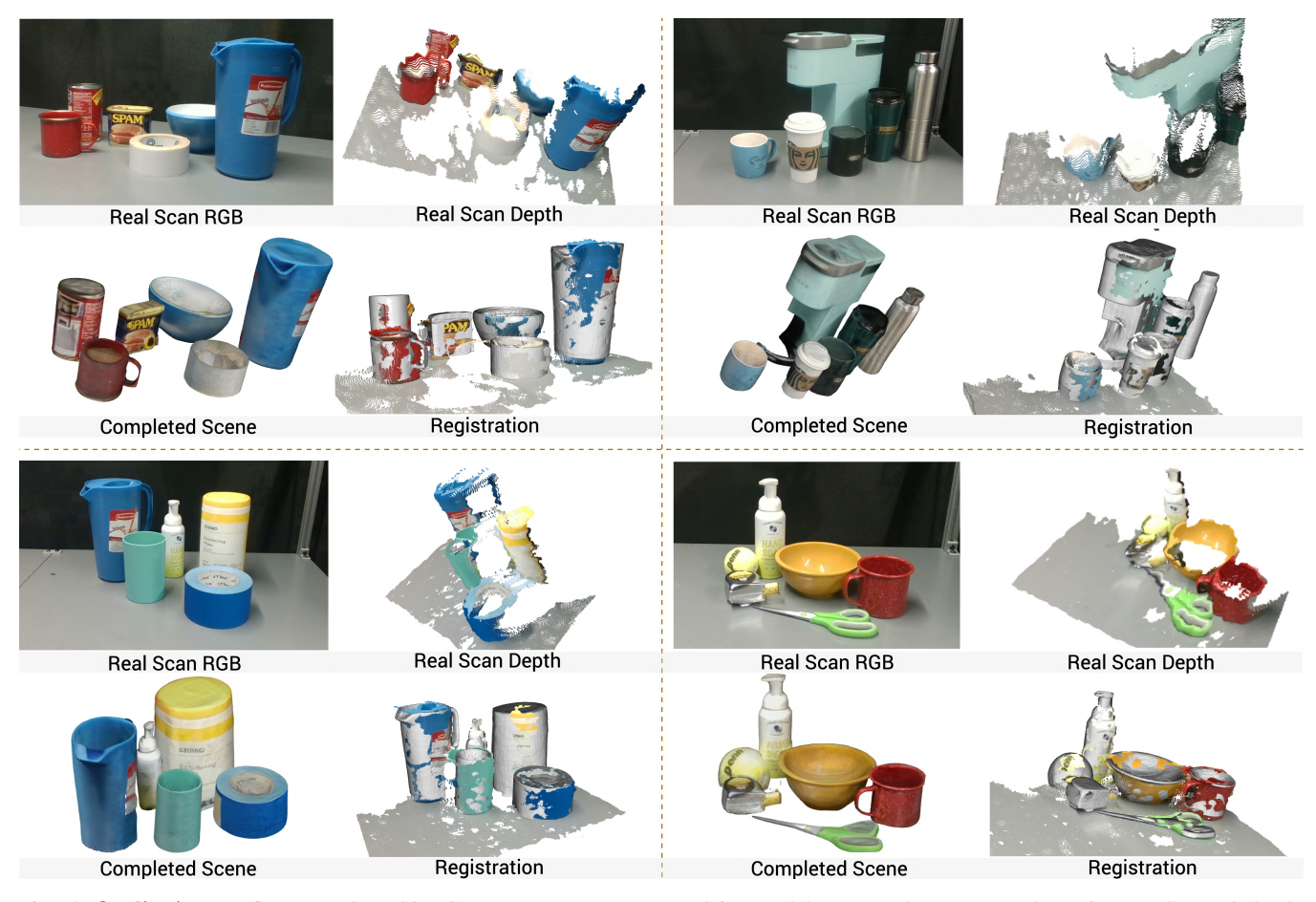


Fig. 5: **Qualitative results** on real-world RGB-D scene scans captured in our lab. For each scene we show: input RGB and depth, the completed scene from a different viewpoint, and a composite of the original point cloud with the completed scene, illustrating the accuracy and registration of the final result. These scenes, composed of arbitrary objects in various configurations, highlight the complexity of real-world environments. As can be seen, *SceneComplete* produces highly detailed 3D scene reconstructions in an open-world setting, despite significant occlusion and clutter, making it ideal for complex robotic manipulation tasks.

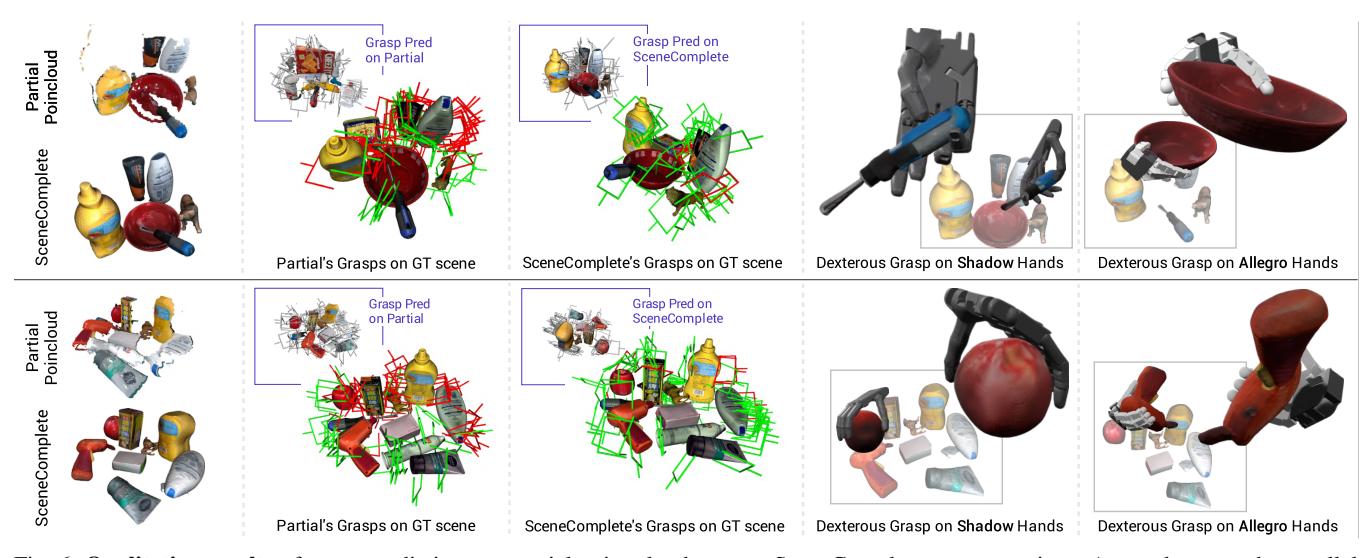


Fig. 6: Qualitative results of grasp predictions on partial point clouds versus SceneComplete reconstructions. As can be seen, the parallel jaw grasps predicted using [13] that samples antipodal grasps on the SceneComplete reconstruction enables more robust predicts with less collisions on the ground truth (GT) scene. We also demonstrate dexterous grasps using both Shadow Hands and Allegro Hands [14], highlighting improved manipulation of complex objects with complete 3D reconstructions.

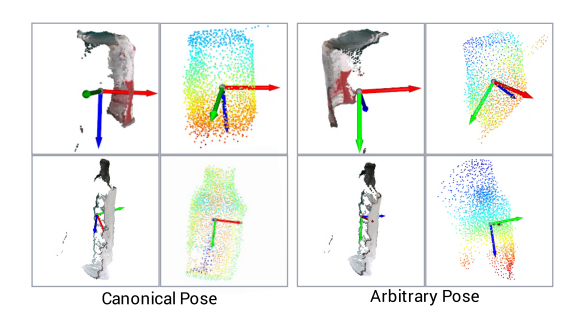


Fig. 7: While impressive, these models [39] struggle with partial observability in real-world depth data even on in-category examples. An underlying assumption is that these models operate on partial inputs in category-specific canonical pose [40].

We evaluated both *SceneComplete* and *SceneComplete*-NoComp (the ablation without 3D shape completion) on all 190 scenes from GraspNet-1Billion and found that *SceneComplete* had an average per-scene IoU score of **0.39** which is more robust, and substantially better than the *SceneComplete*-NoComp's score of **0.14**.

In addition, we performed a basic test of the utility of this model for manipulation by using the antipodal grasping method of DexNet [13] to generate grasps on the objects in the reconstructed scene. To illustrate the importance of whole-scene reconstruction we then ask the question: of these potential grasps, which ones are in collision with other objects? Concretely, for a reconstructed scene, we (a) use DexNet to sample a set G of potential grasps, (b) filter out all grasps in G that would cause a collision in the reconstructed scene to obtain a subset G', (c) filter out all grasps in Gthat would cause a collision in the ground truth scene to obtain a subset G^* , and compute $|G' - G^*|/|G'|$, which is the percentage of grasps that the reconstruction would allow, that in fact collide. We find that, on average over the 190 scenes, only 26% of grasps generated by SceneComplete are in collision with real objects, as opposed to 49% of those generated by SceneComplete-NoComp.

Fig. 6 shows a qualitative analysis of the same. As can be seen, there is a significant reduction in the number of collision of the grasps predicted on the reconstructed scene (*SceneComplete*) in the actual scene (GT scene) than grasps predicted on the partial scene.

B. Dexterous Grasping and Stability

A significant test of the utility of our approach is whether the individual object reconstructions support the computation of good dexterous grasps for a multi-fingered hand. We evaluate each object reconstruction as follows:

- Pass a *reconstructed* object mesh O_i into DexGrasp-Net [14], configured for a dexterous hand (we used both Shadow and Allegro hands), to obtain a grasp g_i .
- Instantiate Isaac Gym [41] with the selected hand and the *ground truth* object mesh.
- Lift the hand within the simulation and detect whether the object is dropped using PhysX as the physics engine.

We tabulate the percentage of such tests that succeed. We selected 20 objects arbitrarily from the Graspnet-1B

dataset and evaluated SceneComplete against SceneComplete-NoComp on the ground-truth object shape (an important upper-bound that illustrates the reliability of Dex-GraspNet for selecting such grasps). We notice that the number of grasps sampled by DexGraspNet varies greatly based on the object geometry. Overall, we observe that DexGraspNet can sample $2\times$ as many valid grasp proposals with SceneComplete than on SceneComplete-NoComp.

IV. DISCUSSION

- a) Limitations: Although our results are very promising, there are of course many failure modes in a composition of so many modules, which can have cascading effects on overall system performance. We outline some failure modes and opportunities for improvement below. Prompting and segmentation: Occasionally the VLM fails to detect some of the object(s) in the image, causing the reconstruction of the object to be missed altogether. Tuning the prompt can mitigate this problem, as can prompting multiple ways for multiple hypotheses. Segmentation: Grounded-SAM occasionally segments parts of an object along with the full object which leads to multiple reconstruction hypotheses for the same object, or detects two cluttered objects together as one. We mitigate this partially using IoU-based de-duplication. **Inpainting:** Our current inpainting strategy operates on a relatively isolated object, which removes some important context. We mitigate this by slightly increasing the bounding box and adapting the model, but there is further room for improvement. Image-to-3D: Although remarkable, these models can sometimes fail to generate plausible reconstructions when given images from highly unusual viewpoints. Scaling and registration: Our scaling method is naive and would be improved in some cases by making it be nonisotropic. Registration sometimes fails on uniformly-textured objects, where it is difficult to find distinctive features. It can also fail if the scaling is incorrect.
- b) Future work: One important strategy for making the system less error-prone is to move to a more generative setting with quantified uncertainty. If each module could generate multiple hypotheses, conditioned on its inputs, it would be possible to search for an interpretation that is collectively satisfactory to all the modules.
- c) Conclusion: We have presented a system that solves full-scene reconstruction from a single real-world RBG-D input in cluttered, occluded scenes with no assumptions about object categories. We have built on an incredibly strong foundation of existing general-purpose open-domain perception models and believe our approach will be able to adapt to and profit from future advances in such models. One goal of this paper is to emphasize the importance of this problem for robot manipulation in real open-world environments and to encourage others to propose alternative solution strategies. We hope that overall advances in scene understanding in realistic manipulation settings will enable much more robust and capable robot manipulation systems.

REFERENCES

- M. Dahnert, J. Hou, M. Nießner, and A. Dai, "Panoptic 3d scene reconstruction from a single rgb image," *Advances in Neural Information Processing Systems*, vol. 34, pp. 8282–8293, 2021.
- [2] L. Mescheder, M. Oechsle, M. Niemeyer, S. Nowozin, and A. Geiger, "Occupancy networks: Learning 3d reconstruction in function space," in *Proceedings of the IEEE/CVF conference on computer vision and pattern recognition*, 2019, pp. 4460–4470. 1, 3
- [3] A.-Q. Cao and R. De Charette, "Monoscene: Monocular 3d semantic scene completion," in *Proceedings of the IEEE/CVF Conference on Computer Vision and Pattern Recognition*, 2022, pp. 3991–4001.
- [4] A. Curtis, X. Fang, L. P. Kaelbling, T. Lozano-Pérez, and C. R. Garrett, "Long-horizon manipulation of unknown objects via task and motion planning with estimated affordances," in 2022 International Conference on Robotics and Automation (ICRA). IEEE, 2022, pp. 1940–1946.
- [5] N. Gothoskar, M. Cusumano-Towner, B. Zinberg, M. Ghavamizadeh, F. Pollok, A. Garrett, J. Tenenbaum, D. Gutfreund, and V. Mansinghka, "3dp3: 3d scene perception via probabilistic programming," *Advances in Neural Information Processing Systems*, vol. 34, pp. 9600–9612, 2021.
- [6] B. Sen, A. Agarwal, G. Singh, B. Brojeshwar, S. Sridhar, and M. Krishna, "Scarp: 3d shape completion in arbitrary poses for improved grasping," in 2023 IEEE International Conference on Robotics and Automation (ICRA). IEEE, 2023, pp. 3838–3845. 1, 3
- [7] S. Peng, M. Niemeyer, L. Mescheder, M. Pollefeys, and A. Geiger, "Convolutional occupancy networks," in *Computer Vision–ECCV* 2020: 16th European Conference, Glasgow, UK, August 23–28, 2020, Proceedings, Part III 16. Springer, 2020, pp. 523–540. 1, 3
- [8] Y. Chen, J. Ni, N. Jiang, Y. Zhang, Y. Zhu, and S. Huang, "Single-view 3d scene reconstruction with high-fidelity shape and texture," in 2024 International Conference on 3D Vision (3DV). IEEE, 2024, pp. 1456–1467.
- [9] S. Popov, P. Bauszat, and V. Ferrari, "Corenet: Coherent 3d scene reconstruction from a single rgb image," in *Computer Vision–ECCV* 2020: 16th European Conference, Glasgow, UK, August 23–28, 2020, Proceedings, Part II 16. Springer, 2020, pp. 366–383.
- [10] A. Dourado, T. E. De Campos, H. Kim, and A. Hilton, "Edgenet: Semantic scene completion from a single rgb-d image," in 2020 25th international conference on pattern recognition (ICPR). IEEE, 2021, pp. 503–510.
- [11] W. Agnew, C. Xie, A. Walsman, O. Murad, Y. Wang, P. Domingos), and S. Srinivasa, "Amodal 3d reconstruction for robotic manipulation via stability and connectivity," in *Proceedings of the 2020 Conference on Robot Learning*, ser. Proceedings of Machine Learning Research, J. Kober, F. Ramos, and C. Tomlin, Eds., vol. 155. PMLR, 16–18 Nov 2021, pp. 1498–1508. [Online]. Available: https://proceedings.mlr.press/v155/agnew21a.html 1
- [12] H.-S. Fang, C. Wang, M. Gou, and C. Lu, "Graspnet-1billion: A large-scale benchmark for general object grasping," in *Proceedings of the IEEE/CVF Conference on Computer Vision and Pattern Recognition*, 2020, pp. 11444–11453. 1, 4
- [13] J. Mahler, M. Matl, V. Satish, M. Danielczuk, B. DeRose, S. McKinley, and K. Goldberg, "Learning ambidextrous robot grasping policies," *Science Robotics*, vol. 4, no. 26, p. eaau4984, 2019. 2, 5, 6
- [14] R. Wang, J. Zhang, J. Chen, Y. Xu, P. Li, T. Liu, and H. Wang, "Dexgraspnet: A large-scale robotic dexterous grasp dataset for general objects based on simulation," in 2023 IEEE International Conference on Robotics and Automation (ICRA). IEEE, 2023, pp. 11359–11366.
- [15] OpenAI, "Chatgpt-4," 2024, large language model, OpenAI. Accessed: September 2024. [Online]. Available: https://openai.com 2
- [16] T. Ren, S. Liu, A. Zeng, J. Lin, K. Li, H. Cao, J. Chen, X. Huang, Y. Chen, F. Yan et al., "Grounded sam: Assembling open-world models for diverse visual tasks," arXiv preprint arXiv:2401.14159, 2024.
- [17] X. Ju, X. Liu, X. Wang, Y. Bian, Y. Shan, and Q. Xu, "Brushnet: A plug-and-play image inpainting model with decomposed dual-branch diffusion," arXiv preprint arXiv:2403.06976, 2024.
- [18] E. J. Hu, Y. Shen, P. Wallis, Z. Allen-Zhu, Y. Li, S. Wang, L. Wang, and W. Chen, "Lora: Low-rank adaptation of large language models," arXiv preprint arXiv:2106.09685, 2021. 3
- [19] S. Mangrulkar, S. Gugger, L. Debut, Y. Belkada, S. Paul, and B. Bossan, "Peft: State-of-the-art parameter-efficient fine-tuning methods," https://github.com/huggingface/peft, 2022. 3

- [20] B. Calli, A. Walsman, A. Singh, S. Srinivasa, P. Abbeel, and A. M. Dollar, "Benchmarking in manipulation research: The ycb object and model set and benchmarking protocols," arXiv preprint arXiv:1502.03143, 2015. 3
- [21] B. Sen, G. Singh, A. Agarwal, R. Agaram, M. Krishna, and S. Sridhar, "Hyp-nerf: Learning improved nerf priors using a hypernetwork," Advances in Neural Information Processing Systems, vol. 36, 2024.
- [22] J. Zhang, X. Chen, Z. Cai, L. Pan, H. Zhao, S. Yi, C. K. Yeo, B. Dai, and C. C. Loy, "Unsupervised 3d shape completion through gan inversion," in *Proceedings of the IEEE/CVF Conference on Computer Vision and Pattern Recognition*, 2021, pp. 1768–1777.
- [23] R. Liu, R. Wu, B. Van Hoorick, P. Tokmakov, S. Zakharov, and C. Vondrick, "Zero-1-to-3: Zero-shot one image to 3d object," in Proceedings of the IEEE/CVF international conference on computer vision, 2023, pp. 9298–9309.
- [24] R. Shi, H. Chen, Z. Zhang, M. Liu, C. Xu, X. Wei, L. Chen, C. Zeng, and H. Su, "Zero123++: a single image to consistent multi-view diffusion base model," arXiv preprint arXiv:2310.15110, 2023. 3
- [25] M. Liu, C. Xu, H. Jin, L. Chen, M. Varma T, Z. Xu, and H. Su, "One-2-3-45: Any single image to 3d mesh in 45 seconds without per-shape optimization," *Advances in Neural Information Processing Systems*, vol. 36, 2024. 3
- [26] M. Liu, R. Shi, L. Chen, Z. Zhang, C. Xu, X. Wei, H. Chen, C. Zeng, J. Gu, and H. Su, "One-2-3-45++: Fast single image to 3d objects with consistent multi-view generation and 3d diffusion," in Proceedings of the IEEE/CVF Conference on Computer Vision and Pattern Recognition, 2024, pp. 10072–10083.
- [27] Y. Hong, K. Zhang, J. Gu, S. Bi, Y. Zhou, D. Liu, F. Liu, K. Sunkavalli, T. Bui, and H. Tan, "Lrm: Large reconstruction model for single image to 3d," arXiv preprint arXiv:2311.04400, 2023.
- [28] D. Tochilkin, D. Pankratz, Z. Liu, Z. Huang, A. Letts, Y. Li, D. Liang, C. Laforte, V. Jampani, and Y.-P. Cao, "Triposr: Fast 3d object reconstruction from a single image," arXiv preprint arXiv:2403.02151, 2024. 3
- [29] J. Xu, W. Cheng, Y. Gao, X. Wang, S. Gao, and Y. Shan, "Instantmesh: Efficient 3d mesh generation from a single image with sparse-view large reconstruction models," arXiv preprint arXiv:2404.07191, 2024.
- [30] B. Poole, A. Jain, J. T. Barron, and B. Mildenhall, "Dreamfusion: Text-to-3d using 2d diffusion," arXiv preprint arXiv:2209.14988, 2022. 3
- [31] H. Wang, X. Du, J. Li, R. A. Yeh, and G. Shakhnarovich, "Score jacobian chaining: Lifting pretrained 2d diffusion models for 3d generation," in *Proceedings of the IEEE/CVF Conference on Computer* Vision and Pattern Recognition, 2023, pp. 12619–12629. 3
- [32] J. Seo, W. Jang, M.-S. Kwak, H. Kim, J. Ko, J. Kim, J.-H. Kim, J. Lee, and S. Kim, "Let 2d diffusion model know 3d-consistency for robust text-to-3d generation," arXiv preprint arXiv:2303.07937, 2023.
- [33] G. Qian, J. Mai, A. Hamdi, J. Ren, A. Siarohin, B. Li, H.-Y. Lee, I. Skorokhodov, P. Wonka, S. Tulyakov et al., "Magic 123: One image to high-quality 3d object generation using both 2d and 3d diffusion priors," arXiv preprint arXiv:2306.17843, 2023. 3
- [34] C.-H. Lin, J. Gao, L. Tang, T. Takikawa, X. Zeng, X. Huang, K. Kreis, S. Fidler, M.-Y. Liu, and T.-Y. Lin, "Magic3d: High-resolution textto-3d content creation," in *Proceedings of the IEEE/CVF Conference* on Computer Vision and Pattern Recognition, 2023, pp. 300–309.
- [35] S. Amir, Y. Gandelsman, S. Bagon, and T. Dekel, "Deep vit features as dense visual descriptors," arXiv preprint arXiv:2112.05814, vol. 2, no. 3, p. 4, 2021. 3
- [36] A. Dosovitskiy, "An image is worth 16x16 words: Transformers for image recognition at scale," arXiv preprint arXiv:2010.11929, 2020.
- [37] M. Caron, H. Touvron, I. Misra, H. Jégou, J. Mairal, P. Bojanowski, and A. Joulin, "Emerging properties in self-supervised vision transformers," in *Proceedings of the IEEE/CVF international conference* on computer vision, 2021, pp. 9650–9660.
- [38] B. Wen, W. Yang, J. Kautz, and S. Birchfield, "Foundationpose: Unified 6d pose estimation and tracking of novel objects," in *Proceedings of the IEEE/CVF Conference on Computer Vision and Pattern Recognition*, 2024, pp. 17868–17879.
- [39] P. Xiang, X. Wen, Y.-S. Liu, Y.-P. Cao, P. Wan, W. Zheng, and Z. Han, "Snowflakenet: Point cloud completion by snowflake point deconvolution with skip-transformer," in *Proceedings of the IEEE/CVF* international conference on computer vision, 2021, pp. 5499–5509.

- [40] J. Zhang, X. Chen, Z. Cai, L. Pan, H. Zhao, S. Yi, C. K. Yeo, B. Dai, and C. C. Loy, "Unsupervised 3d shape completion through gan inversion," in *Proceedings of the IEEE/CVF Conference on Computer Vision and Pattern Recognition*, 2021, pp. 1768–1777. 6
 [41] J. Liang, V. Makoviychuk, A. Handa, N. Chentanez, M. Macklin, and D. Fox, "Gpu-accelerated robotic simulation for distributed reinforcement learning." in Conference on Polyet Learning. PMI P. 2018, pp.
- ment learning," in Conference on Robot Learning. PMLR, 2018, pp. 270–282. 6